International Journal of Sensors and Sensor Networks
2023; 11(1): 1-10
http://www.sciencepublishinggroup.com/j/ijssn
doi: 10.11648/j.ijssn.20231101.11
ISSN: 2329-1796 (Print); ISSN: 2329-1788 (Online)

Preventive Work and Health Monitoring for Technology by Cracks of Concrete Surface Using Coating Type Resin Sensor

Nobuhiro Shimoi[1, *], Yu Yamauch[1], Kazuhisa Nakasho[2]

[1]Faculty of Systems Science and Technology, Akita Prefectural University, Yurihonjo, Japan

[2]Graduate School of Sciences & Technology for Innovation, Yamaguchi University, Ube, Japan

Email address:

Shimoi@akita-pu.ac.jp (Nobuhiro Shimoi), yamauchi.yu@akita-pu.ac.jp (Yu Yamauch), nakasho@yamaguchi-u.ac.jp (Kazuhisa Nakasho)

[*] Corresponding author

To cite this article:

Nobuhiro Shimoi, Yu Yamauch, Kazuhisa Nakasho. Preventive Work and Health Monitoring for Technology by Cracks of Concrete Surface Using Coating Type Resin Sensor. *International Journal of Sensors and Sensor Networks*. Vol. 11, No. 1, 2023, pp. 1-10.
doi: 10.11648/j.ijssn.20231101.11

Received: April 7, 2023; **Accepted**: May 8, 2023; **Published**: May 18, 2023

Abstract: Infrastructure safety inspections rely on visual inspections and hammering inspections by inspectors. However, an important difficulty is that inspection results vary because of differences in the technical expertise of inspectors. An inspection method and preventive work using a coating type resin sensor and an infrared camera are proposed to overcome that difficulty. A nondestructive evaluation technique using thermography is used increasingly as a tool to maintain concrete structures. Most inspections only evaluate the defect locations and shapes on planes. No method has been developed for evaluating defect depths. After applying infrared reactive resin, thermographic images of a target area are taken sequentially. Then, temperature curves obtained at each pixel during cooling defect states in different parts of the temperature distribution are analyzed using Fourier transform. The temperature change is related to the defect size. Approximately 10% of aluminum powder mixed into the applied gel resin, because of its specific gravity, has the property of concentrating in areas damaged by compression failure or floating. This report describes technologies related to defect identification and size measurements in infrared reactive resin, and describes effects of preventive work to avoid the scattering and collapse of defects caused by structural degradation.

Keywords: Infrared Thermography, Non-Destructive Inspection, Reinforcement, Spalling Prediction, Health Monitoring

1. Introduction

In Japan, many infrastructurally important structures such as bridges and tunnels have been produced for more than 50 years [1]. In 20 years, 65% of bridges and 45% of tunnels are expected to be over 50 years old. Monitoring technology to verify the soundness of structures is therefore crucially important to monitor deterioration and structural changes constantly under long-term monitoring. Such monitoring also plays an important role in constructing the system. In the past, safety inspections of infrastructure structures were targeted within 50 years after construction, when safety was assured. In practical terms, bridges that have already reached the end of their useful life must continue to be used. It therefore becomes necessary to detect dangerous conditions, such as their structural collapse, as soon as possible. Long-term monitoring of deterioration and structural changes constantly is important because such changes strongly affect social safety and security. Realization of such monitoring can be supported by measurement and evaluation methods after fully elucidating aspects of the usage environment, such as the characteristics of the structure to be measured and its duration of use. The development of new monitoring technologies is therefore urgently necessary. To realize such monitoring of structural integrity, one must fully understand the characteristics of the structure to be measured and the usage environment such as the number of years of use. Then one can consider measurement and evaluation methods before implementing them. Maintaining the soundness of infrastructure reliably requires accurate evaluation of the state of structures by judging the presence, frequency, and location of damage from survey and inspection data.

Specifically, we quantify empirical evaluation methods such as “visual inspection” and “hammering inspection.” Further improvement of the efficiency of “nondestructive inspections” such as X-ray inspection and magnetic flaw detection (standardization, cost reduction, etc.) and high performance (improvement of accuracy, automatic data judgment, etc.) are important [2].

Therefore, the authors have developed a method to measure the soundness of concrete piers of bridges, inner walls of tunnels, tiled walls of high-rise buildings in a simple, long-term, inexpensive manner, to identify anomalies such as concrete cracks, defects, and wall floats. A technical method was examined. Our findings suggest that the problem can be resolved using the original infrared reactive resin and image analysis technology that enables passive measurement using a long-wave infrared camera. This technology is based mainly on active measurement such as heating and pre-cooling because of temperature changes of the measurement object, which are usually measured using an infrared camera. To enable passive measurement at room temperature (21°C), we mixed aluminum powder into the gel resin and applied it to the concrete to be treated. When a crack occurs on the concrete wall surface shown in Figure 1(a) or when a float shown in Figure 1(b) occurs, the aluminum powder in the gel resin flows and concentrates at the defect. Therefore, after the wall retains heat from sunlight, the missing part is highlighted by the temperature difference between the infrared radiation and the atmosphere. Furthermore, even if no heat radiation from sunlight is incident on the wall surface, detecting defects and anomalies from the temperature difference between the wall surfaces is possible because of differences in materials: a radiative cooling effect is created by the aluminum powder in the gel resin. That effect can be read as a representative signature.

In addition, the coated gel resin for this measurement has a repair effect: it flows into cracks and defects because of differences in specific gravity between the resin and metal. Therefore, this measurement method is regarded as a measurement technology serving both as a measure of defects in concrete walls and as a preventive measure. Reportedly, rainwater flowing into the concrete structure from a defective area flows into gaps and causes rain leakage, thereby accelerating deterioration [3]. As described herein, concrete test specimens were created to verify the developed technology. Results of investigations of the crack emergency capacity and measurement effects of this resin sensor by destructive testing are reported. In recent years, methods using an external camera have been applied to measure "float" and "surface cracks" related to reinforcing steel corrosion in concrete. However, the radiant energy of infrared rays is proportional to the temperature. An infrared camera detects the infrared energy and converts it into a pseudo-temperature image. The detection wavelength of infrared rays is probably approximately equal to the middle infrared wavelength. The density of heat energy is expected to increase as the wavelength decreases.

(a) (b)

Figure 1. *Concrete flaking occurs, cracking the concrete surface.*

2. Preventive Work and Measurement Technology Using an Infrared Reactive Coating Type Resin Sensor

In recent years, external cameras have been used to measure "float" and "surface cracks" related to reinforcing steel corrosion in concrete. However, the radiant energy of infrared rays is proportional to the temperature. An infrared camera detects the infrared energy and converts the results of the detection into a pseudo-temperature image. The density of heat energy is expected to increase as the wavelength [4–5].

2.1. Comparison with Conventional Technologies

Various methods are used for the quantitative evaluation of structural soundness for disaster prevention and mitigation. Regarding sensor systems for measuring displacement and vibration because of static loading, a method exists for measuring displacement using a laser displacement meter or a contact-type displacement meter, as well as a method of measuring natural vibration with a micro vibration meter and then analyzing the fracture state and stress concentration using FEM analysis. Methods exist to identify such locations [6–7]. In addition, X-ray analysis using FEM is useful as a non-destructive and quantitative evaluation method for residual stress in structures, but analyzing crack growth using this method is difficult. Among these methods, microtremor vibration measurements obtain the Fourier spectrum ratio of vertical and horizontal motion components [8], normalize the horizontal vibration to the vertical vibration, and determine the amplification characteristics and natural period of the structure. Other methods might also be used to obtain the natural period of the structure.

The measurement system consists of a microtremor meter, a data logger, and a PC. Laser Doppler velocimetry (LDV) [9] detects velocity from the phase difference based on the Doppler Effect between the irradiated light and the reflected light when the object is irradiated with laser light. This measurement system consists of two LDV devices, a data logger, a PC, and a digital displacement gauge. Such devices cost about 4.5 to 6 million yen (34.6–46.1 thousand US dollars) per measurement unit. Alternatively, non-destructive X-ray equipment can be installed for the monitoring of limited areas, but such devices are not practical for long-term

measurement because they require equipment costs of about 8–10 million yen and a high-capacity and reliable power supply. However, for wall inspection technology of structures using an infrared camera, the thermography method, which uses the temperature difference created by sunlight on the outer wall of the building, uses differences in the conductivity of the wall material to measure differences that occur in the defective part [10]. Additionally, we have developed a technique using an image filter processing method that emphasizes the damaged area from an infrared thermal image and a statistical establishment method for estimating the probability of damage prediction as an index of the degree of damage in the temperature change part based on the feature value of the processed image [11].

In addition, Nakamura et al. of Kyoto University used infrared thermography to measure specimens at each damage stage in a reinforcement corrosion expansion pressure simulation test for the quantitative evaluation of the spalling risk. The degree of risk of spalling is calculated as an index that is adequate to support evaluation of the degree of deterioration irrespective of the form [12–13].

To evaluate concrete structures' safety and soundness, long-term monitoring during more than 20 years is regarded as necessary. However, the difficulty exists that neither a measuring device able to guarantee the required monitoring period nor a smart sensing method that enables danger prediction exists at present [12, 14–17]. Table 1 presents specifications of the infrared camera used for measurement. Figure 2 portrays an image of the camera used for testing.

Table 1. *Specifications of the infrared camera.*

Model	InfRec R450; Nippon Avionics Co. Ltd.
Detector	Two-dimensional non-cooling method
Measurement temperature range	-40 to 1500 °C
Measurement wavelength	8 to 14 μm
Number of pixels	480 × 360
Measurement field of view	24 degrees × 18 degrees
Standard lens	10 cm to ∞
Weight	3.8 kg

Figure 2. *IR Camera.*

2.2. Principle of Infrared Thermography

Objects that exist at room temperature emit energy by infrared radiation. Planck's law of radiation is expressed in equation (1), which states that an object emits energy proportional to the fourth power of its absolute temperature. Boltzmann's law is presented in equation (2) [18].

$$E(\lambda T) = \frac{2hc^2}{\lambda^5}\frac{1}{e^{hc/\lambda KT}-1}[\mathrm{W/(m^2\mu m)}] \quad (1)$$

$W\lambda b$: Black body spectral radiant emittance at wavelength λ
c: Speed of light 3 × 108 [m/s]
h: Planck's constant (6.6×10^{-27} Js)
K: Boltzmann's constant (1.38×10^{-16} J/k)
T: Absolute temperature of blackbody (K)
Λ: Wavelength (m)

$$Wb = \sigma t^4 \ [\mathrm{W / m^2}] \quad (2)$$

Wb: Integrating wavelength from λ = 0 to λ＝∞ from Planck's formula.
Black body spectral radiance −8 2(W・$\mathrm{SR^{-1}m^2}$)
σ: Boltzmann's constant (5.7 × 10 W/m)
t: Absolute temperature of blackbody (K)

$$\lambda_{max} = 2897/T \ [\mu m] \quad (3)$$

When the measurement target is 40°C (absolute temperature T = 273 + 40 = 313 K), wavelength λ is 2897 ÷ 313 = approximately 9.2 μm from equation (3).

2.3. Infrared Thermal Radiation Relational Expression

Figure 3 portrays an image acquired using infrared thermal radiation. The infrared rays emitted from the measurement target are propagated by equations (4)–(6). From the principle of the infrared thermography method, when measured using an infrared camera indoors, if no difference exists between the outside temperature in the air and the temperature of the test object, then the heating of the test object must also be considered. We compare changes in the infrared thermal images with and without preheating. Moreover, we measure the effects of applying gel resin under similar conditions [19].

$$(1-\varepsilon) \times W(Ta) \quad (4)$$

$$\varepsilon \times W(T) \quad (5)$$

$$\varepsilon < 1 \quad (6)$$

T: Object temperature
E: Spectral radiant heat of the object
Ta: Temperature of the facing surface

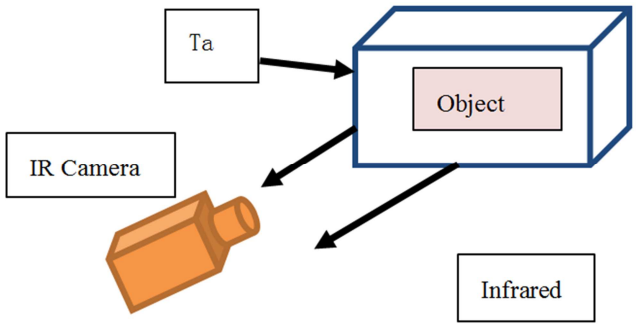

Figure 3. *Image acquisition by infrared thermal radiation.*

3. Measurement Method and Performance Evaluation of Infrared Reactive Coating Type Resin

3.1. Image Analysis Using an Infrared Reactive Coated Resin Sensor

From the principle of the infrared thermography, when measuring with an infrared camera indoors, if no difference exists between the outside temperature in the atmosphere and the temperature of the test object, then one can forcibly heat the surface, perhaps using a halogen lamp, to heat the interior of the test object. A method of measuring cracks and floats based on the temperature difference between the surface and interior can be used. However, the use of such a method requires that the measurement conditions always be established and implemented under favorable conditions, with due consideration devoted to the influence of the outside air temperature, the measurement target material and color, the spectral reflectance, and the measurement distance. Actual practical measurements are expected to be difficult. Figure 4 portrays the influence of the loading tester of the specimen (a) and the reinforcement arrangement of the specimen (b). A test specimen is prepared using ordinary concrete with a 2 cm cover thickness on this reinforcing bar. For this study, to improve the measurement level considering the problems caused by these thermal image characteristics, specimen A was an RC post with a φ65 hole drilled 23.5 cm below the center on the left side of the lower part of the specimen (a). Specimen (b) is an RC post with a φ65 hole drilled 235 mm above the center on the right side of the specimen.

A hole of φ65 was artificially machined to imitate the defect of a concrete support column. It was conducted to measure the strength effects on the upper and lower parts. However, to ascertain the measurement effects of the infrared camera by resin coating and the result of preventive work in the fracture situation, gel-like resin (CY52-276; Dow Corning Toray Co. Ltd.) was applied to the entire lower surface of each test body AB, except for the upper 300 mm. A coating film containing 1% aluminum powder with particles of 10–20 μm was applied to about 0.1 mm thickness. The material properties of this resin include resistance to ultraviolet rays, lack of hardening over time in the coating film, and maintenance of a gel-like property. Moreover, it does not retain water. It takes about 1 hr to harden after mixing 1 liquid and 2 liquids equally. The price is 1,000 yen per kilogram.

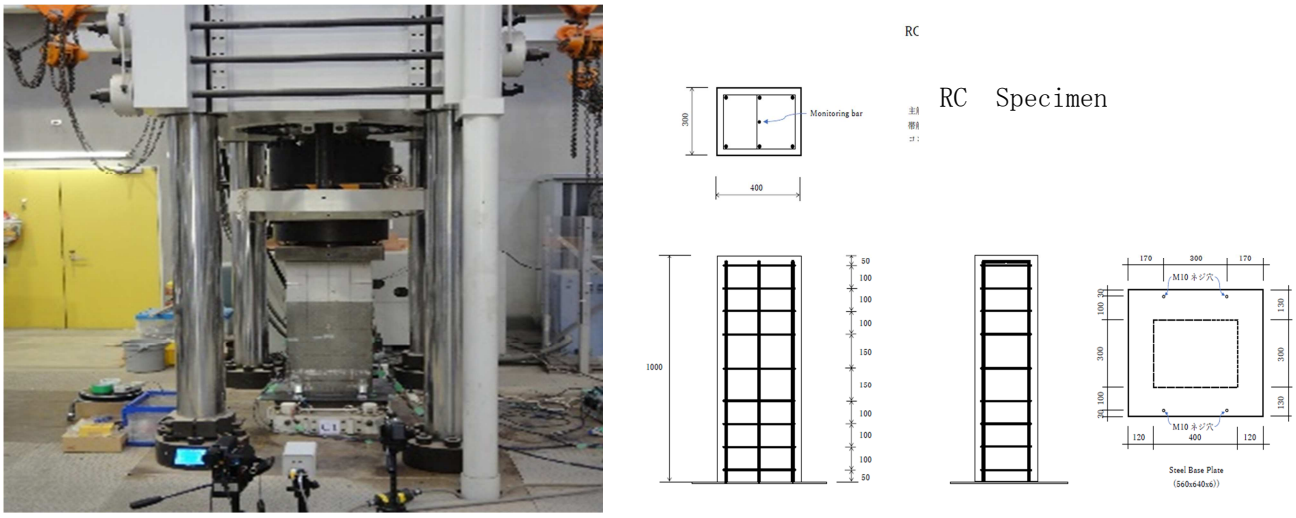

(a) (b)

Figure 4. *Experiment of equipment and specimen.*

3.2. Infrared Imaging Using Resin Coating

(1) Examination of thermal image analysis by passive measurement

To compare the effects of thermal imaging with and without surface overheating, specimen A was heated from the back side for about 20 min using a carbon heater (900 W; Yamazen Corp.). Because the thermal conductivity of concrete is 1.6, about 61.05 times higher than the thermal conductivity of air, which is 0.026, we predicted that the surface temperature would rise after about 30 min. Therefore, after another 30 min had passed, we conducted a destructive test. Figure 5 presents temperature changes of specimens (a) and (b). Panel (a) shows a temperature comparison of specimen (a) by measurement with overheating. Panel (b) presents the measurement results found for specimen (b) measured at room temperature (21°C) without overheating by passive measurement. The temperature difference on the surface of the specimen from the start to the end of the test was 4°C for (a) and 0.6°C for (b). Figure 6 portrays details of the position and shape of the through-holes made in specimens (a) and (b).

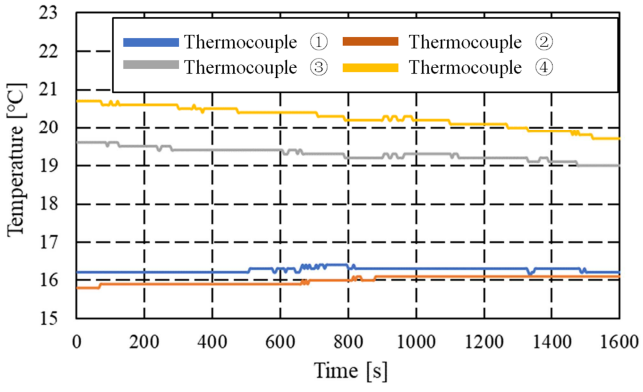

(a)

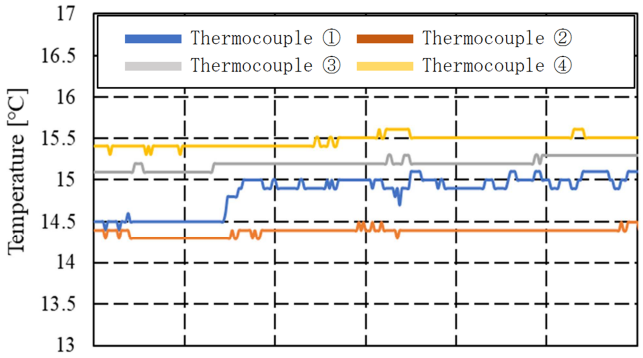

(b)

Figure 5. *Relation of temperature difference in specimens a and b to the temperature change of the specimens.*

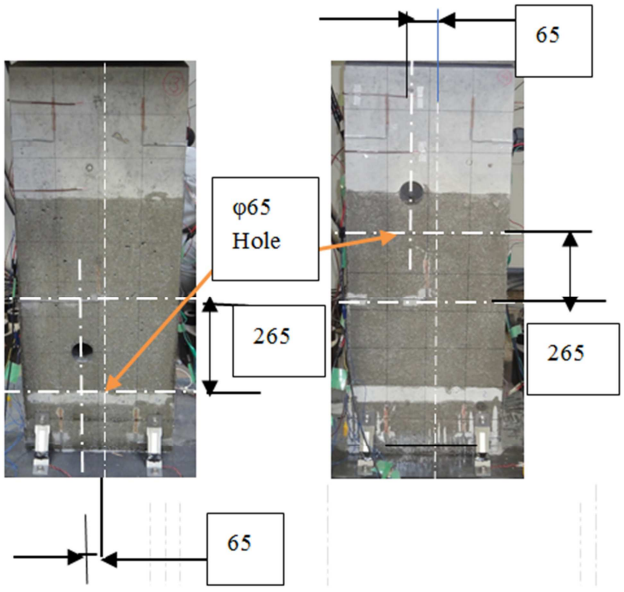

(a) (b)

Figure 6. *Specimen (a) and Specimen (b) (size 300 × 400 × 1000 mm).*

(2) Evaluation of preventive construction work

On specimens (a) and (b), the gel-like resin (CY52-276; Dow Corning Toray Co., Ltd.) was applied to the entire lower surface, except for the upper 300 mm at about 0.1 mm thickness. We observed the damage and the state of falling fragments after the destructive testing of the parts coated with this resin and parts not coated with this resin. Figure 7 presents specimen (b) after completion of the destructive test. Destruction is generated by the shearing force generated obliquely from the right side of the screen and compressive force applied from the top. Particularly, it seems that infrared measurement was able to confirm the effects of suppressing the scattering and collapse of concrete fragments because of compression failure and the "floating" situation indicated by the arrow, which is difficult to detect using a visible-light camera. Panel (a) depicts a thermal image of Specimen B taken using an infrared camera. Panel (b) portrays an image taken using a visible-light camera. In both cases, the elapsed times of force application were equal.

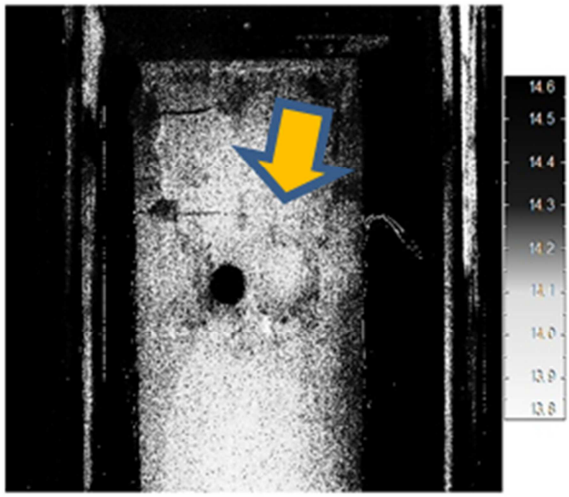

(a)

(b)

Figure 7. *Infrared camera image and visible-light camera image.*

4. Measurement Results and Discussion

4.1. Infrared Images Compared by Application of Gel Resin

Figure 8 presents results obtained from the destructive tests conducted on specimens with upper and lower defects.

Panel (a) presents a comparison of (1) an infrared thermal image and (2) a visible-light image at the time of maximum load, and (3) an infrared thermal image and (4) a visible-light image at the end of loading, for the specimen in Figure 6(a) with preheating. Panel (b) presents the (1) infrared thermal image at maximum load and (2) visible-light image, (3) infrared thermal image at the end of loading and (4) visible-light image of the specimen in Figure 6(b) without preheating. Panel (c) shows (1) an infrared thermal image at maximum load and (2) a visual comparison of the visible-light image with the optical image, and (3) the infrared thermal image at the end of loading.

In panel (a), the test was started 30 min after heating the test piece with a carbon heater for 20 min. As shown in Figure 9, the temperature was measured and recorded (1) at the center 50 mm from the top of the surface, (2) at the center 250 mm from the top of the surface, (3) at the center 50 mm from the top of the back, and (4) at the center 250 mm from the top of the back. The infrared thermal image reproduces a state in which the upper temperature is high and the lower temperature is low. In the visible-light image, the state of damage caused by the load applied to the test object is recognized only on the surface, but in the infrared thermal image, the damage state of the surroundings directly affected by the applied force in the deep part is also recognized. Our findings demonstrated the possibility of observing invisible parts in contrast to visible-light images. The temperature difference of the specimen was confirmed as matching the theory-based prediction: The residual heat strongly affected the external thermal image of the specimen surface after a certain period of time. Figure 8(b) presents a comparison of the infrared thermal image (1) and visible-light image (2) under the maximum load, and the infrared thermal image (3) and visible-light image (4) after the end of the load at room temperature of 21°C with no preheating. In the infrared thermal image, as Table 2 shows, the temperature difference of the specimen is only 0.6°C, but it is recorded in a state that is comparable to the image after heating shown in (a). This finding is attributable to the effects of the resin applied to the specimen surface. The resin has effect of a poultice and maintains the difference between the temperature of the specimen surface and room temperature, making it possible to obtain clear infrared thermal images [4].

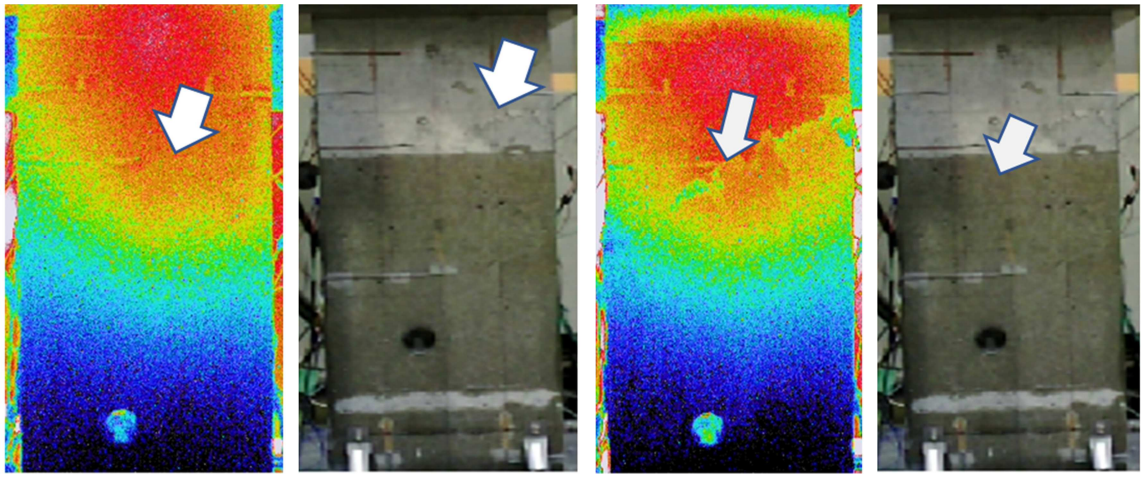

(1) (2) (3) (4)

(a)

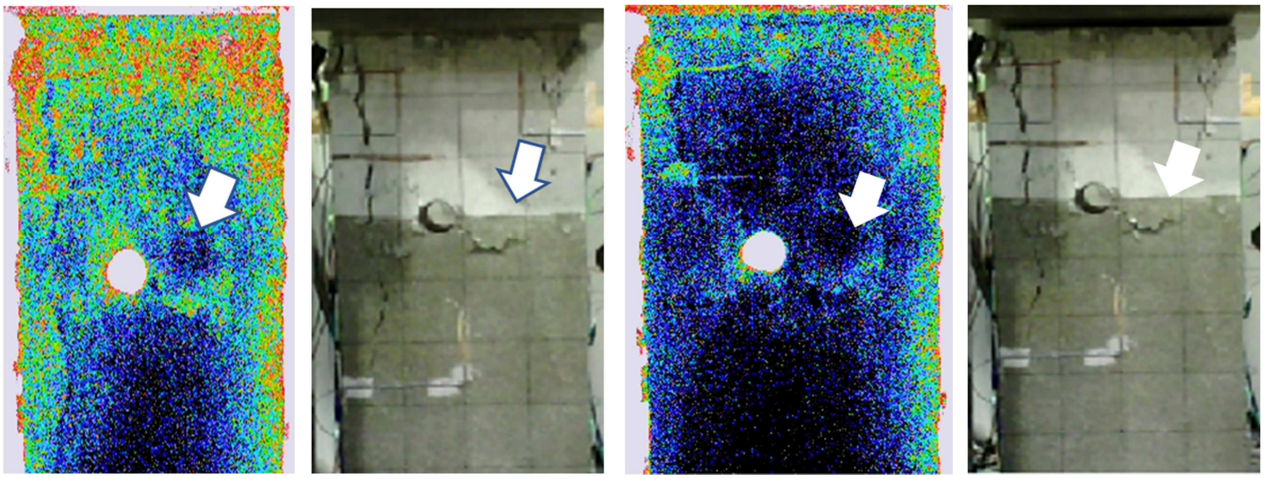

(1) (2) (3) (4)

(b)

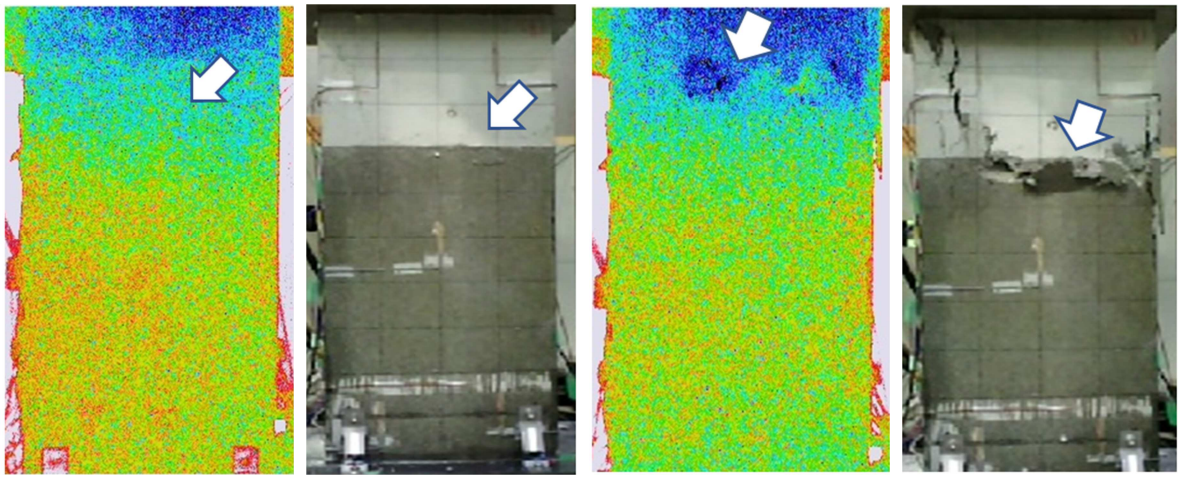

(1) (2) (3) (4)

(c)

Figure 8. *Results of destructive tests conducted on specimens with upper and lower defects and non-defects.*

Figure 8 (c) portrays a comparison of the infrared thermal image (1) and visible-light image (2) under maximum load, and an infrared thermal image (3) and visible-light image (4) after the end of loading at room temperature without preheating, with no defect. In the infrared thermal image, although the results shown in Table 2 present the temperature difference of the specimen as only 0.8°C, it is recorded in a state that is comparable to the image after heating shown in (a). The effects of the resin applied to the surface were clearly divisible into two in the thermal image. Results demonstrated that the temperature was maintained at a low temperature.

4.2. Examination of Preventive Work by Gel Application Resin

As Figure 9 shows, the results of the destructive tests on specimens with comparison of upper and lower defects show that the fracture conditions of both specimens (a) and (b) exhibit that fractures progress greatly in the central part of the specimen. In addition, (c) is characterized by the structural strength: The damage of specimen (b) with a defect in the upper part is greater than that in the specimen (a) with a defect in the lower part. Figure 9 presents results obtained from measuring the relation between stress and strain on specimens (a), (b), and (c) in time series, and measuring the results at five locations. In the graph, strain is shown as a light blue solid line. Force is represented by a blue dashed line. As shown in (6), the strain on the specimen surface was measured at five points from top to bottom, from (1)–(5). In addition, Table 3 presents results obtained from measuring the strain at each maximum load at the measurement positions on the surface of each specimen shown in (6) in Figure 9. As these results show, when stress is applied from above, structural strength is lost because of compressive failure and shear failure: destruction progresses from the top. Strain is concentrated in the center. Specimen (a) with a hole in the lower part did not exhibit any characteristic such as a noteworthy loss of strength or progression of structural failure. Cracks did not occur to the lower part. From the start, the specimen withstands a maximum load of 2500 kN for about 20 min. However, specimen (b) with a hole in the upper part was found to have no endurance, reaching a maximum load of 2000 kN in about 12 min. In the state of fracture, the strain increased from the top. The maximum strain was recorded at the central portion at 3000 μm. Particularly, the fracture progressed radially from the defect hole perimeter. In fact, the left side of the test specimen had a large vertical crack from the top to the bottom with approximately 4–8 mm width. Under these conditions, results showed that specimen (b) had less physical strength than specimen (a). Moreover, the fracture was larger. Specimen (c) displays the result of a compression test with no fracture. Actually, it is the strongest in terms of physical strength. However, in terms of the damage size and depth, a tendency was apparent by which the damage was concentrated in the central part of the specimen with intentional defects. Regarding the resin effect, the effect of swelling prevention was observed on both sides of the specimen.

Even under such conditions, areas coated with gel resin showed inhibited fracture progress and reduced crack depth and size. Regarding the application of gel resin, a certain effect was observed. It is probably effective at preventing collapses inside tunnels and at preventing falling objects because of age-related deterioration of concrete bridge piers.

Table 2. *Measurement surface temperature gaps by specimens (a), (b) and (c).*

Strain No.	Test specimen a (°C)	Test specimen b (°C)	Test specimen c (°C)
(1)	16.3	14.9	14.5
(2)	16.0	14.4	15.0
(3)	19.3	15.2	15.2
(4)	20.3	15.5	15.3
Temperature gap	4	0.6	0.8

Table 3. *Measurement strain gaps and times to the peak by specimens (a), (b) and (c).*

Strain No.	Test specimen a Strain (μm)	Time (s)	Test specimen b Strain (μm)	Time (s)	Test specimen c Strain (μm)	Time (s)
1	2500	1200	2250	700	2500	1417
2	1500	1200	2600	700	2500	1618
3	1000	1200	3000	750	500	1367
4	500	900	500	750	1000	1252
5	500	400	750	750	800	1260
gap	2000	800	2500	50	2000	366

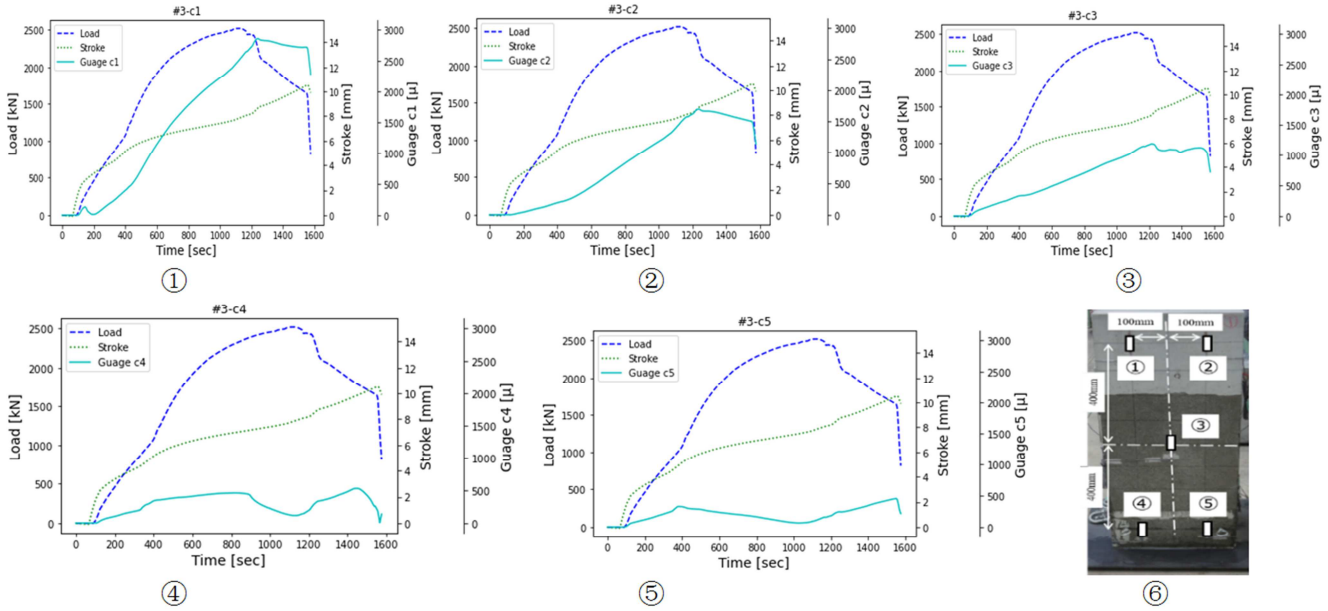

(a)

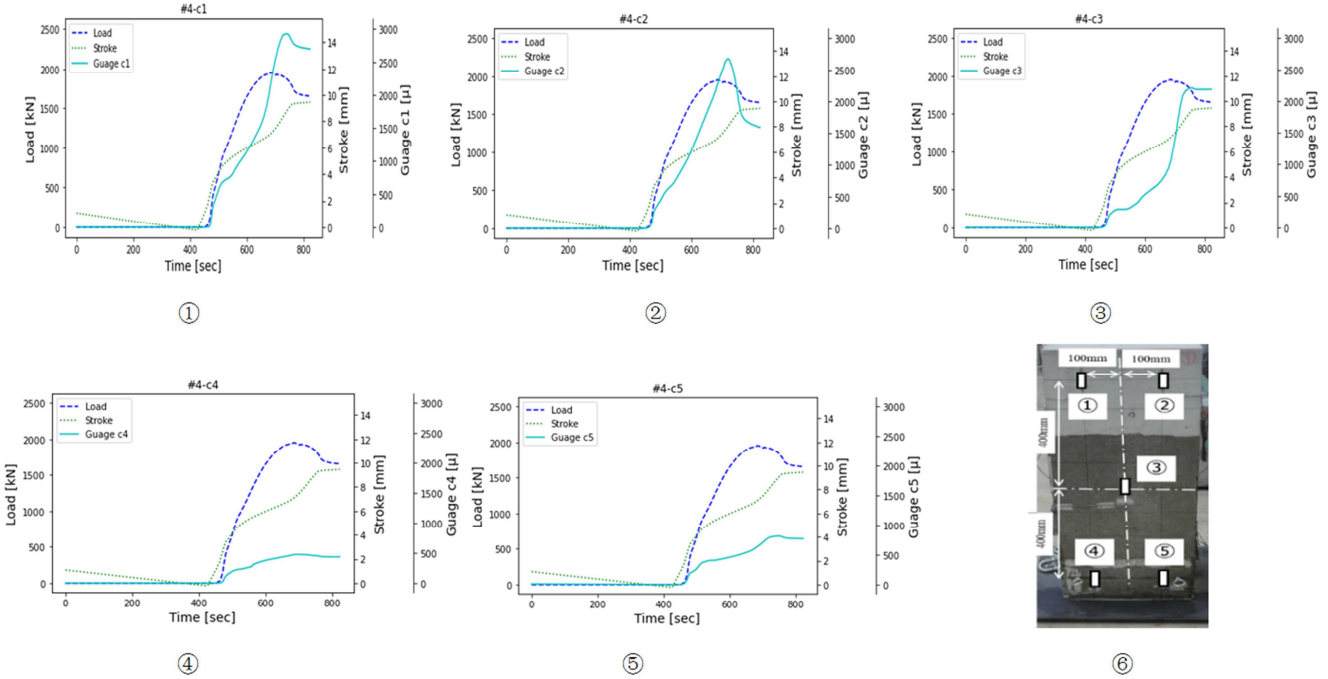

(b)

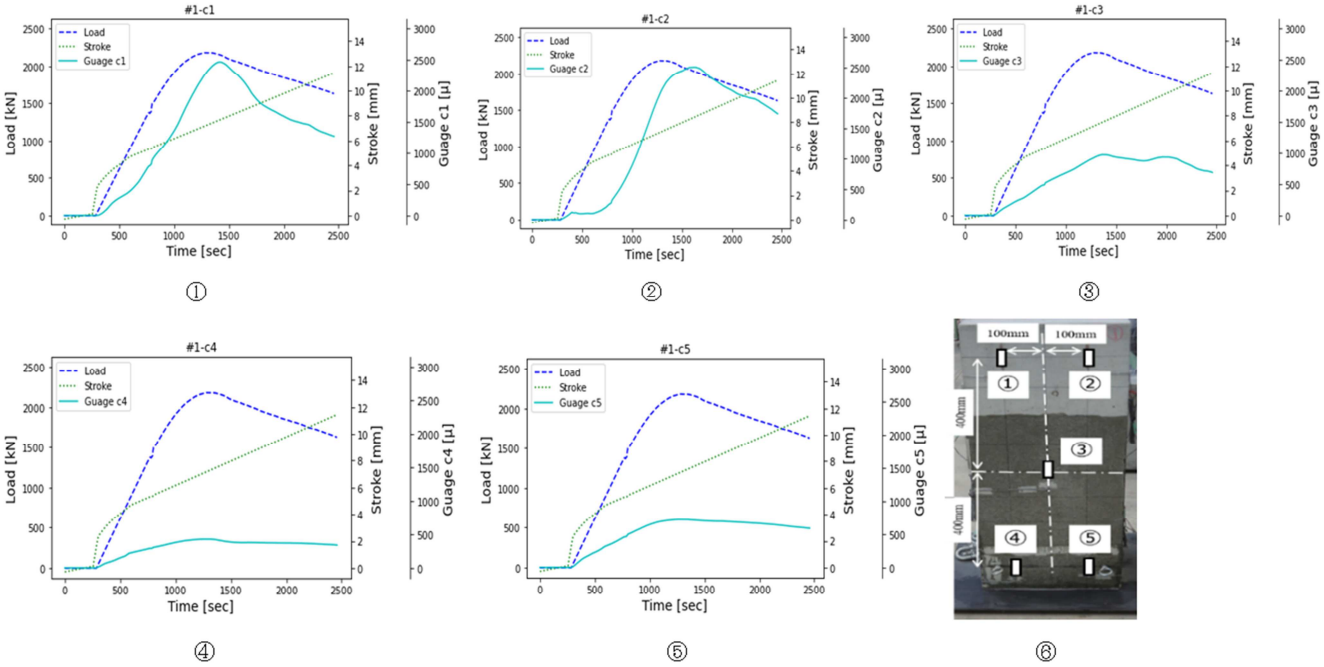

(c)

Figure 9. *Relation between strain load and non-defects on the specimen surface.*

5. Conclusion

Using this measurement technology, this study produced the following findings.

1) Improving the resolution of infrared thermal images necessitates an increase of the temperature difference from outside air. Effects of the Planck's law principle were confirmed. Clear thermal images were obtained while maintaining a large radiant heat difference from the fracture site. In this case, because of the relation between the heat conduction ratio of concrete, even if heat generation from the outside is performed, the thermal image effect cannot be obtained unless sufficient time has elapsed.
2) Reportedly, shear failure occurs first from compression, but that could not be verified by this test because of the relation to the press velocity. IR thermal image measurements confirmed that the central part bulges to the left and right because of the test piece expansion. Measurements taken using visible light made it possible to visualize parts that are difficult to confirm.
3) Because urethane resin is hard and vulnerable to deterioration when exposed to ultraviolet rays, the gel resin coating improves thermal image acquisition during passive measurement. Results suitable for measuring "peeling" and "floating" were obtained.
4) By virtue of the protective effects of the resin coating, it was confirmed as useful for construction to prevent fracture and peeling progress during fracture. Additionally, it was found to be effective for preventing debris from the top and for avoiding the fall and collapse of the fracture site.
5) To prevent cracks in structures and to prevent the corrosion of reinforcing bars, rainwater must be prevented from entering. The effects of applying the resin are thought to prevent rainwater ingress and to prevent metal corrosion and deterioration.
6) Infrared thermal imaging showed that the surface coating effect of this resin was effective at suppressing swelling and surface peeling caused by deformation of the reinforced concrete column during loading.

Acknowledgements

We thank Dr. Hiroshi Fukui, Senior Research Scientist of Dow – Toray Co. Ltd. and Mr. Takashi Harasaki, Commercial Manager of Dow Toray Co. Ltd., for providing test materials and expert advice about resins. This research was partially supported by JSPS Kakenhi Grant No. 20H00290, for which we express our appreciation.

References

[1] Ministry of Land, Infrastructure, & Transport. Infrastructure maintenance information. Available from <https://www.mlit.go.jp/sogoseisaku/maintenance/02research/02_01_01.html> (accessed on 10 October, 2020). (in Japanese).

[2] Matsuoka, H., Hirose, Y., Kurahashi, T., Murakami, Y., Toyama, S., Ikeda, H., Iyama, T. & Ihara, I. (2018) Application of a joint variable method for high accurate numerical evaluation of defect based on hammering test. Journal of the Society of Materials Science, Vol. 67, No. 9, pp. 869-876. (in Japanese).

[3] Ueda, H., Ushijima, S. & Shyutto, K. (2007) Properties and deterioration prediction of acid attacked concrete. Japan Society of Civil Engineers, Vol. 63 No. 1, pp. 27-41 (in Japanese).

[4] Xu, J., Wang, H, Duan, Y., He, Y., Chen, S. & Zhang, Z. (2020) Terahertz imaging and vibro-thermography for impact response in carbon fiber reinforced plastics. Infrared Physics & Technology, pp. 1-18.

[5] Wu, D., Haude, C., Burger, R. & Peters O. (2019) Application of terahertz time domain spectroscopy for NDT of oxide–oxide ceramic matrix composites. Infrared Physics & Technology, Vol. 102, pp. 1-9.

[6] Tamai, H. (2003) Elasto Plastic Analysis Method for frame with exposed-type column base considering influence of variable axial force. Journal of Structural and Construction Engineering, Vol. 68, No. 571, pp. 127-135. (in Japanese).

[7] Shimoi, N., Nishida, T., Obata, A., Nakasho, K., Madokoro, H. & Cuadra, C. (2016) Comparison of displacement measurements in exposed type column base using piezoelectric dynamic sensors and static sensors. American Journal of Remote Sensing, Vol. 4, No. 5, pp. 23-32. (in Japanese).

[8] Nagao, T., Yamada, M. and Nozu, A., A study on the empirical evaluation method of site amplification effects by use of microtremor H/V spectrum, JSCE Committee of Structural Engineering, Vol. 56A (2010), pp. 324–333 (in Japanese).

[9] Miyashita, T., Ishii, H., Fujino, Y., Shoji, T. & Seki, M. (2007) Understanding of high-speed train induced local vibration of a railway steel bridge using laser measurement and its effect by train speed. Japan Society of Civil Engineering A, Vol. 63, No. 2, pp. 277-296 (in Japanese).

[10] Michimura, K. (2008) Deterioration diagnosis technology by infrared method. Material Life Society, Vol. 20, No. 1, pp. 21-26 (in Japanese).

[11] Hayashi, H., Hashimoto, K. & Akashi, Y. (2013) Improving detection accuracy of concrete damage by infrared thermography. Japan Concrete Institute, Vol. 35, No. 1, pp. 1813-1818 (in Japanese).

[12] Nakamura, M. (2002) Health monitoring of building structures. Society of Instrument and Control Engineers, Vol. 41, No. 11, pp. 819-824 (in Japanese).

[13] Shimoi, N. (2001) The technology of personal mine detecting for humanitarian demining. SICE, Vol. 37, No. 6, pp. 577-583 (in Japanese).

[14] Ono, K. (2003) Study on technology for extending the life of existing structures, New Urban Society Technology Fusion Research. The Second New Urban Social Technology Seminar, pp. 11-23 (in Japanese).

[15] Wan, M., Gu, G., Qian, W., Ren, K., Chen, Q., Zhang, H. & Malgague, X. (2018) Total variation regularization term-based low-rank and sparse matrix representation model for infrared moving target tracking. Remote Sensing, Vol. 10, No. 510, pp. 1-22.

[16] Luo, Q., Gat, B., Woo, W. L. & Yang, Y. (2019) Temporal and spatial deep learning net work for infrared thermal defect detection. NDT and E International, pp. 1-13.

[17] Kumagai, K., Nakamura, H. & Kobayashi, H. (1999) Computer aided nondestructive evaluation method of welding residual stresses by removing reinforcement of weld. Transactions of the Japan Society of Mechanical Engineers, Series A, Vol. 65, No. 629, pp. 133-140 (in Japanese).

[18] Shimizu, K. (1987) The latest technology for far-infrared use. Industrial Technology Association, pp. 6-24 (in Japanese).

[19] Malgague, X. (2002) Introduction to NDT by active infrared thermography. Materials Evaluation, pp. 1-22.